Chalcogenide Letters Vol. 11, No. 10, October 2014, p. 493 - 502

TUNING STRUCTURAL AND ELECTRONIC PROPERTIES OF MoS_2 NANOTUBES BY TRANSVERSE ELECTRIC FIELD

Y.Z. WANG[a], B.L. WANG[b], Q.F. ZHANG[b,e], R. HUANG[a], B.L. GAO[a], F.J. KONG[c], X.Q. WANG[d, *]

[a]*Department of Applied Physics, Huaiyin Institute of Technology, Jiangsu, 223003, China*

[b]*Key Laboratory for Advanced Technology in Environmental Protection of Jiangsu Province, Yancheng Institute of technology, Jiangsu, 224051, China*

[c]*Department of Physics, Yancheng Institute of Technology, Jiangsu, 224051, China*

[d]*Department of Physics,Jinling Institute of Technology, Nanjing, Jiangsu, 211169, China*

[e]*Laboratory of Solid State Microstructures, Nanjing University, Nanjing 210093, China.*

The structural and electronic properties of MoS_2 nanotubes (NTs) under the transverse electronic field are investigated by density functional theory calculations. Under the transverse electric field, the circular cross-sections of the MoS_2 NTs are deformed to elliptic, the band gap of the MoS_2 NTs almost linearly decreases with increasing the strength of electric field, and the modulation of the structure and band gap is dependent on the tube diameter. It is also found that a suitable critical transverse electric field could induce the semiconductor-metal transition in MoS_2 NTs. Furthermore, the electric field can tune the effective mass of the carriers of the MoS_2 NTs.

(Received September 1, 2014; Accepted October 8, 2014)

Keywords: MoS_2 nanotube, electric field, band structure, density functional theory

1. Introduction

Molybdenum disulfide (MoS_2) is a unique semiconductor (1.2 eV) with a typical layered honeycomb structure like graphite, which offers many distinct electronic, mechanical, optical and catalytic properties[1].

It is well known that the MoS_2 can be formed a variety of different nanostructures with unique properties, which make them have many potential applications, such as lubricants[2], catalysis[3], transistors[4], sensors[5], photoemitting devices[6], hydrogen storage[7], and Li-ion batteries[8]. For example, different from the indirect band gap for the bulk MoS_2, monolayer MoS_2 is the direct band gap of 1.9 eV[6], which is favorable for optoelectronic applications. Zigzag MoS_2 nanoribbons show the ferromagnetic and metallic behavior, while the armchair nanoribbons are nonmagnetic and semiconducting[9]. Zigzag MoS_2 NTs are direct semiconductor, while the armchair MoS_2 NTs exhibit indirect semiconductor[10]. Among these nanostructures, MoS_2 NTs have attracted a considerable research interest due to their potential use as the fundamental building blocks for microelectronic and optoelectronic nanodevices.

*Corresponding author: wangxq@jit.edu.cn

As is well known, band gap engineering of MoS_2 NTs could lead to new functionalities in these materials. Among several strategies currently being employed to engineer band gaps in other nanostructures, the band gap tuning by the external electric field have been a subject because that the electric field is expected to significantly alter the electronic and mechanical properties of those nanostructures and propose important applications. Previous studies have proved that the electric field can efficiently modulate the electronic properties of the carbon NTs[11-13], SiC NTs[14], BN NTs[15,16], GaN NTs[17], ZnO nanowires and NTs[18,19], AlN nanoribbons[20], MoS_2 nanosheet and nanoribbons[21-23]. However, to the best of our knowledge, the influence of the electric filed on the MoS_2 NTs is still lack.

In this work, we systematically investigated the structures deformation and the band gap variation of the armchair and zigzag MoS_2 NTs under the transverse electric field. We found that the radial deformation and the band gap variation of the MoS_2 NTs are dependent on the electric field strength and the tube diameter. Furthermore, a suitable critical transverse electric field could induce the semiconductor-metal transition, and the electric field can tune the effective mass of the carriers.

2. Computational methods

In this work, all the calculations were carried out within the framework of density functional theory (DFT) implemented in the $DMol^3$ package[24,25]. The exchange-correlation interactions were described by the generalized gradient approximation (GGA) of the Perdew-Burke-Ernzerhof (PBE) parameterization[26]. Density functional semicorepseudopotentials[27] and double numerical plus polarization (DNP) basis sets were employed.

The MoS_2 NTs were treated within supercell under the periodic boundary conductions. The direction of the tube axis is along the *z* axis of the supercell (see Fig. 1), and the direction of the electric field is along the *x* axis (perpendicular to the tube axis). To eliminate the interaction between MoS_2 NTs in adjacent supercells, the vacuum spaces were set as four times of the diameters of the NTs along the *x* and *y* directions. Geometrical optimization was performed with the converge criteria of maximum Hellmann-Feynman force acting on each atom less than 0.002 hartree/Å and the change of the total energy less than 10^{-5} hartree between two steps. The 1D Brillouin zone (BZ) sampling with Monkhorst-Pack (MP) method of 1×1×11 k-points were chosen during geometry optimization, and thirty k points were sampled for computing the 1D electronic structure.

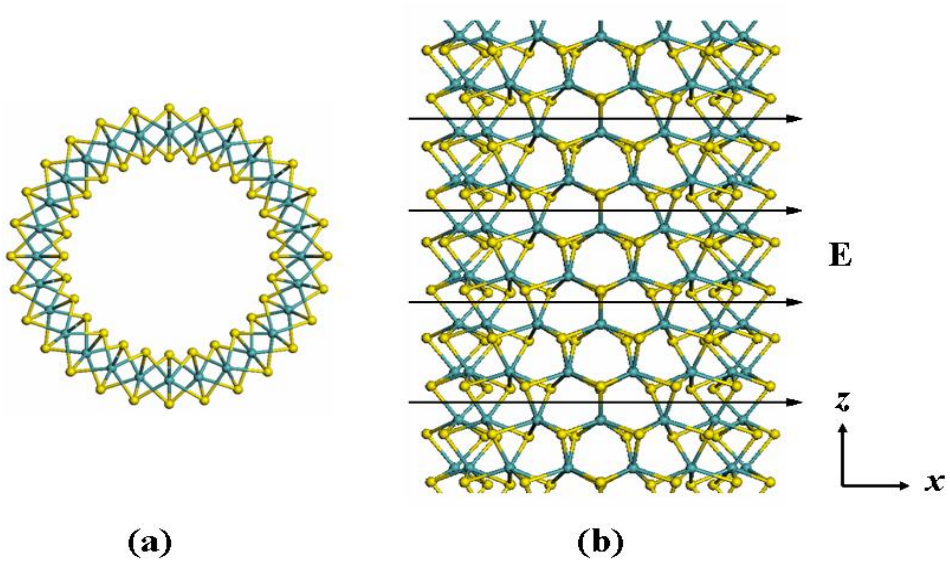

Fig. 1. (a) The topview of the (14, 0) MoS_2 nanotube, (b) the sideview of the (14, 0) nanotube. The green atom stands for Mo, and the yellow atom is S. The arrow indicates the direction of the electric field

3. Results and discussion

Without the electric field, the optimized values of the lattice constant (tube diameter) for (10, 0), (14, 0), (8, 8), (10, 10) MoS_2 NTs are 5.35Å (11.61 Å), 5.44Å (15.34 Å), 3.21 Å (14.93 Å), and 3.21 Å (18.29 Å), respectively, which is consistent with the previous results[28]. Under the sufficiently strong transverse electric field, we found the obviously deformation of the MoS_2 NTs along the direction of the electric field. The inset in Fig. 2 is the deformed (14, 0) nanotube under the transverse electric field of 0.014 a.u.. One can see that the diameter along the direction of the electric field is elongated, whereas the diameter perpendicular to the electric field is lessened, therefore the circular cross-sections of the nanotubes are deformed to elliptic ones under the electric field. To characterize the degree of deformation of the MoS_2 NTs under the electric field, we calculated the aspect ratio (D_{maj}/D_{min}) of the nanotubes. The D_{maj} and D_{min} represent the major diameter and minor diameter of the ellipse cross-section, respectively, as shown in the inset of the Fig. 2. From the Fig. 2, we can see that the aspect ratio is small under the weak electric field, while it gradually increases with increasing the electric field strength. We also found that the radial deformations for the large diameter nanotubes with the same chirality are more severe under the same electric field. At the same time, we found the radial deformation of the (10, 10) nanotube is more obvious than that the (14, 0) nanotube at the same electric field, though the diameter of (10, 10) nanotube is smaller than that the (14, 0) nanotube, indicating the radial deformations of armchair MoS_2 NTs are more easy than that the zigzag MoS_2 NTs.

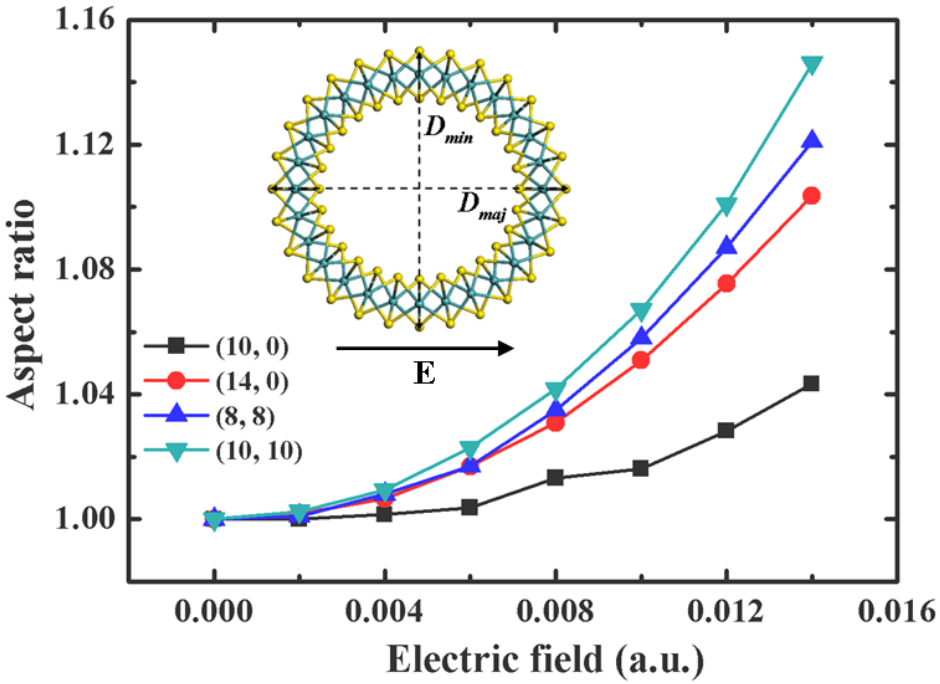

Fig.2. The aspect ratio (D_{maj}/D_{min}) of the nanotube with different diameters under different electric field strength. The inset shows the structure of the deformed (14, 0) nanotube under the electric field of 0.014 a.u.. The direction of the arrow is the direction of the electric field

Fig. 3 shows the band structures of the (14, 0) and (10, 10) MoS_2 NTs under the different electric fields. As shown in Fig. 3(a) and 3(d), we first calculated the band structures of the (14, 0) and the (10, 10) MoS_2 NTs without the electric field. We found the (14, 0) MoS_2 nanotube exhibit a direct band gap ($E_g = 0.72$ eV) consisting of the valence band maximum (VBM) and the conduction band minimum (CBM) both at the Γ point, and the (10, 10) MoS_2 nanotube possesses the indirect band gap ($E_g = 0.93$eV) with the VBM and CBM at between the Γ and Z, which is consistent with the previous report[10]. Under the electric field of 0.01 a.u., the band gaps of the (14, 0) and (10, 10) MoS_2 NTs reduce to 0.26 eV and 0.29 eV, respectively. At the same time, we also found the band gaps of the (14, 0) and (10, 10) MoS_2 NTs remain respectively the direct gap and indirect gap under the electric field, the sites of the VBM and CBM almost remain unchanged, as shown in the Fig. 3(b) and 3(e). Interestingly, in Fig. 3(c) and 3(f), we found that the semiconductor to metal transitions for the (14, 0) and the (10, 10) NTs are induced under the electric field of 0.018 a.u..

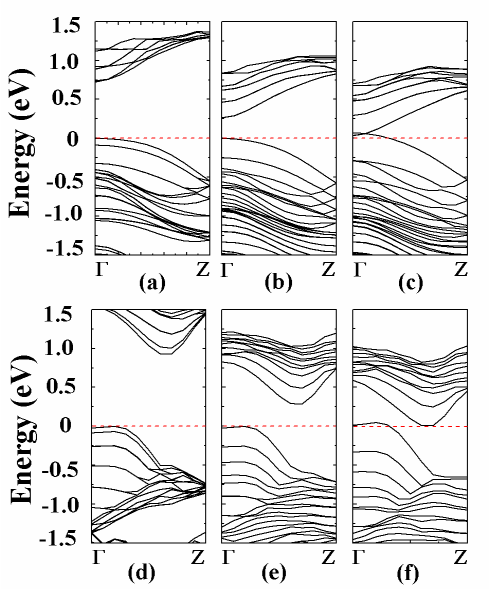

Fig. 3. Band structure of the (14, 0) MoS_2 nanotube under the transverse electric field of (a) 0, (b) 0.01 a.u., (c) 0.018 a.u., respectively; band structure of (10, 10) MoS_2 nanotube under the transverse electric field of (d) 0, (e) 0.01 a.u., (f) 0.018 a.u., respectively. The Fermi level is hinted by the red dash line.

To further investigate the reasons for the reduction of the band gap under the electric field, we study the highest occupied molecular orbital (HOMO) and the lowest unoccupied molecular orbital (LUMO) of the (14, 0) MoS_2 nanotube with and without the electric field, respectively, as shown in Fig. 4. For the (14, 0) MoS_2 nanotube under the zero field, the HOMO is uniformly distributed at the Mo and outer S atoms along the circumferential direction, while the LUMO is mainly concentrated at the Mo atoms along the circumferential direction. When the electric field is applied, the HOMO and LUMO are redistributed along the electric field direction due to the break of electrostatic potential symmetry, which is known as the giant Start effect (GSE)[29]. As shown in Fig. 4(c) and 4(d), the HOMO and LUMO are localized the opposite side along the direction of the electric field, so the electrostatic potential of the charge is raised (HOMO) or lowed (LUMO). The redistribution of the HOMO and LUMO induces the splitting of sub-bands near the Fermi level and further narrowing of the band gap[23,29].

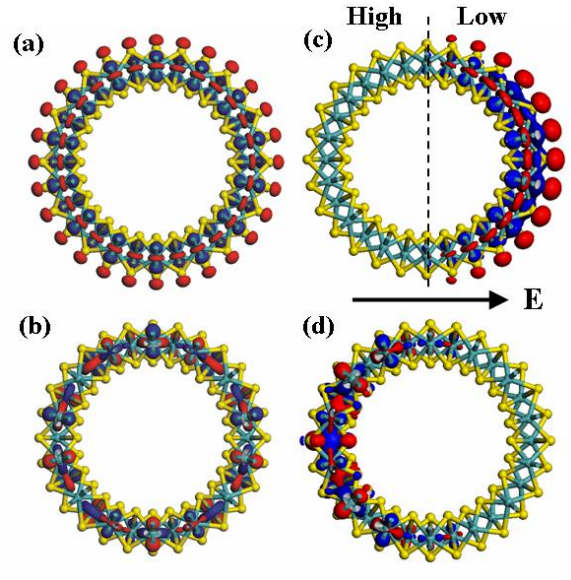

Fig. 4. The (a) and (b) are the highest occupied and the lowest unoccupied molecular orbitals (HOMO and LUMO) of the (14, 0) nanotube under the zero electric field; The (c) and (d) are the HOMO and LUMO of the (14, 0) nanotube under the electric field of 0.01 a.u..The high and low potential regions in the nanotube are separated by the dash line. (isovalue 0.02 e/Å)

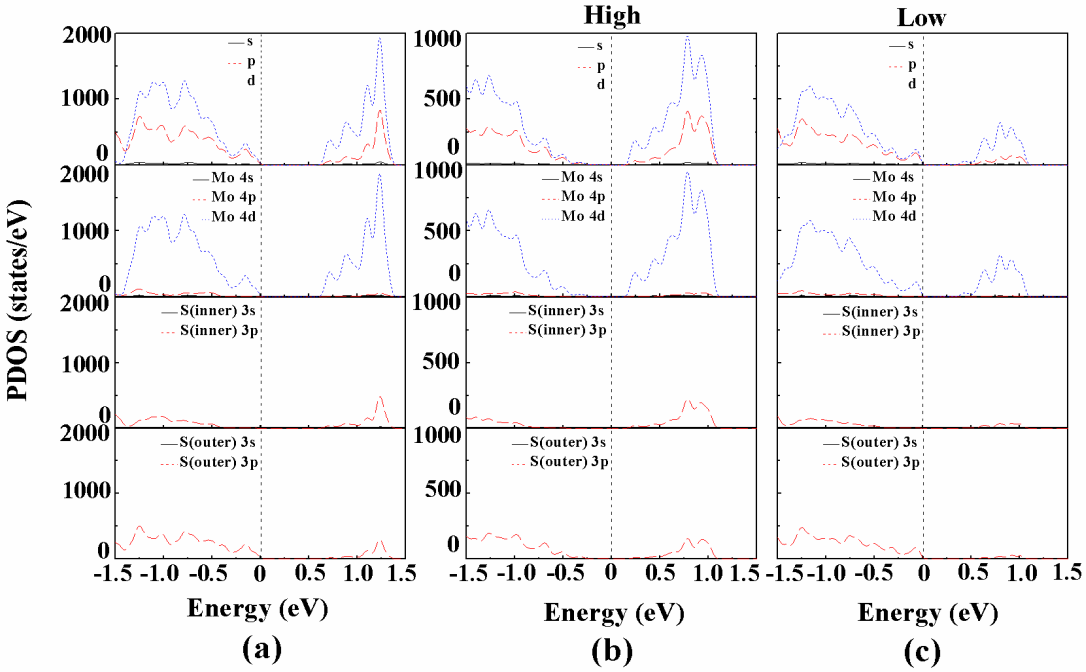

Fig. 5 (a) The partial density of states (PDOS) of (14, 0) MoS_2 nanotube without the electric field and the PDOS in the high(b), and low(c) potential region under the electric field of 0.01 a.u.. The Fermi level is indicated by the dash line.

To further understand the effect of electric field on the electronic properties of the MoS_2 NTs. We plot the partial density states (PDOS) of the (14, 0) MoS_2 nanotube without electric field and the PDOS in high and low potential region (showing in the Fig. 4(c)) under the electric field of 0.01 a.u. in Fig. 5. From Fig. 5(a), we can observe that the VBM of MoS_2 nanotube comes from the 4*d* state of the Mo atoms and the 3*p* state of the outer S atoms, while the CBM is mainly contributed by the 4*d* state of the Mo atoms. At the same time, under the electric field, the VBM comes from the 4*d* state of the Mo atom and the 3*p* state of the outer S atoms in the low potential region, and the CBM is mainly contributed from the 4*d* state of the Mo atom in the high potential region. These results are consistent with the analysis in Fig. 4. Comparing Fig. 4(a)-4(c), it can be seen that the CBM in high potential region is nearer to Fermi level, the VBM in low potential region and the CBM in high potential region will result in the reduction of the band gap under the electric field. Furthermore, in Fig. 6, we show the total density of states (TDOS) of (14, 0) MoS_2 nanotube in high and low potential regions under the electric field of 0, 0.01 a.u. and 0.018 a.u., respectively. Comparing the electronic states under the different electric field as shown in Fig. 6, we can see that the VBM shift toward low energy direction under the electric field, the larger shift is expected by the stronger electric field, which will result in the reduction of the band gap, especially, the semiconductor-metal transition will happen when the CBM in the high potential region cross the Fermi level under the critical electric field.

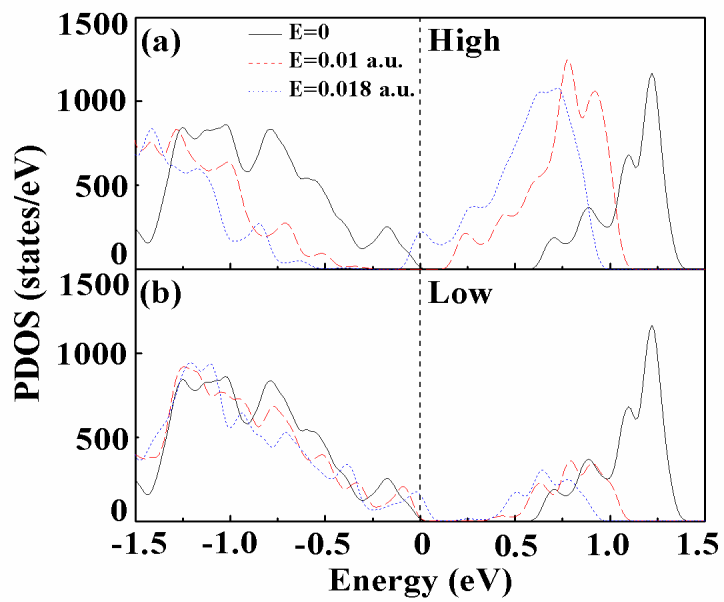

Fig. 6. The total density of states (TDOS) of the (14, 0) MoS_2 nanotube in the high(a) and low(b) potential regions under the external electric field. The Fermi level is indicated by the dash line.

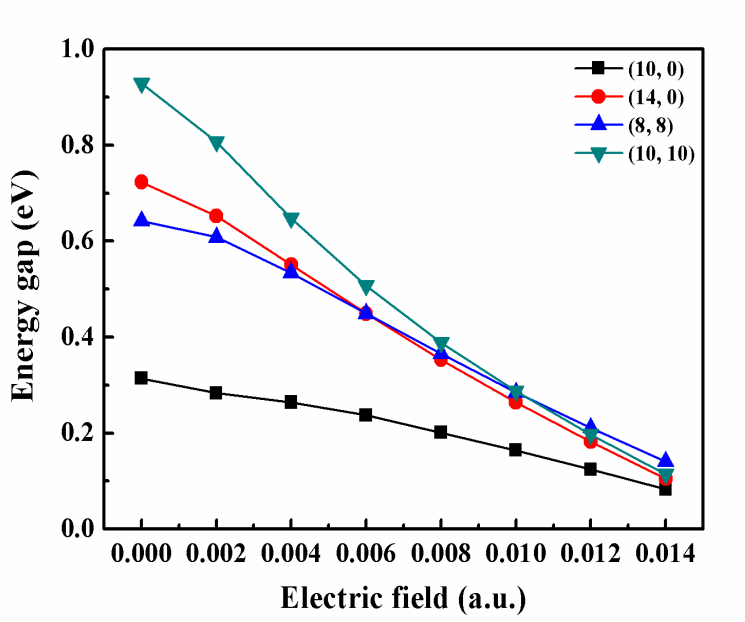

Fig. 7. The band gap of (10, 0), (14, 0), (8, 8), and (10, 10) nanotubes as function of the electric field strength.

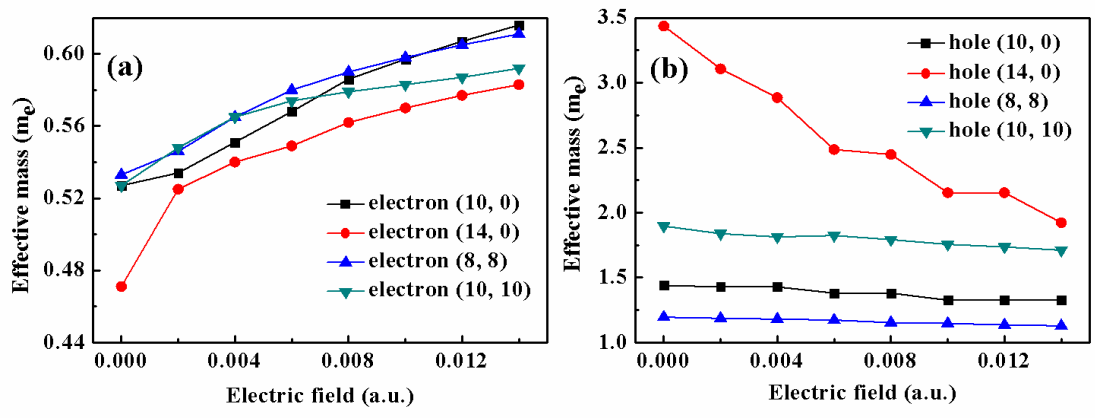

Fig. 8. The effective mass (in units of the free electron mass m_e) of the electron (a) and hole (b) for different MoS_2 NTs under the different electric field strength.

To analyze the effects of diameter and chirality of the MoS_2 NTs, we plot the variations of the band gap for the MoS_2 NTs with different diameters and chiralities under various electric fields, as shown in Fig. 7. In general, the reductions of the band gaps are almost linear with the increasing of the electric field strength, and this trend does not depend on chirality of the tube. While the reductions of the band gaps are faster for the larger diameter NTs under the given electric field. So we can engineer easily the band gaps for the larger diameter NTs with the smaller electric field, which make the MoS_2 NTs as the promising candidates for the optoelectronic device application.

The effective mass of the carriers is one of the most important physical quantities for the device applications. It can be calculated by $m^* = \hbar[d^2E(k)/dk^2]$, where $E(k)$ is the energy

band, k is the coordinate vector in the reciprocal space, and $\hbar$ is the reduced Planck constant[30]. The effective masses of the electron and hole with respect to the different electric fields are shown in Fig. 8. Under the zero electric field, the effective masses of the electron (hole) for the (10, 0), (14, 0), (8, 8) and (10, 10) are 0.527 (1.44) m_e (m_e is the mass of a free electron), 0.471 (3.437) m_e, 0.533 (1.195) m_e and 0.527 (1.896) m_e, respectively, and the holes have the larger effective mass than the electrons for all different MoS_2 NTs, which is consistent with the previous paper[28,31]. In general, for different NTs, the electron effective mass increases with the increasing of the electric field, on the contrary, the hole effective mass decreases; the variation of the effective mass of the carriers are not sensitive to the chirality. The larger variation of the effective mass under the electric field demonstrates the possibility of tuning the mobility of the MoS_2 NTs and help to design the electronic nanodevices.

4. Conclusions

In conclusion, by first-principles calculations we have systematically investigated the structure deformation, electronic properties and the effective mass of the carriers of the MoS_2 NTs under the electric field. The radial deformation of NTs is dependent on not only the tube diameter but also the tube chirality. The band gap of the MoS_2 NTs almost linearly decreases with increasing the electric field, and the variation is enhanced as the tube diameter is increased, which is not sensitive to the tube chirality, especially, a suitable critical transverse electric field could induce the semiconductor-metal transition. Furthermore, the electric field can efficiently modulate the electron and hole effective mass. These results would be helpful to design the future electronic and optoelectronic nanodevices.

Acknowledgements

This work was supported by the Foundation for the National Natural Science Foundation of China (11474246, 11174242, 11404279, 11174101 and 11204265)，the research fund of Key Laboratory for Advanced Technology in Environmental Protection of Jiangsu Province (AE201125) and the Natural Science Foundation of Jiangsu Province (NSFJS, No. BK2012248 and 13KJ430007), and sponsored by Qing Lan Project and 333 project of Jiangsu province, and supported by Science Foundation of Jinling Institute of Technology (jit-rcyj-201403).

References

[1] X.F. Song, J.L. Hu, H.B. Zeng, J. Mater. Chem. C **1**, 2952 (2013).
[2] M. Mosleh, N.D. Atnafu, J.H. Belk, O.M. Nobles, Wear **267**, 1220 (2009).
[3] J. Kibsgaard, A. Tuxen, K.G. Knudsen, M. Brorson, H. Topsøe, E. Laegsgaard, J.V. Lauritsen, F. Besenbacher, J. Catal. **272**, 195 (2010).

[4] B. Radisavljevic, A. Radenovic, J. Brivio, V. Giacometti, A. Kis, Nat. Nanotech. **6**, 147 (2011).
[5] D. Sarkar, W. Liu, X.J. Xie, A.C. Anselmo, S. Mitragotri, K. Banerjee, ACS Nano **8**, 3992 (2014).
[6] K.F. Mak, C.G. Lee, J. Hone, J. Shan, T.F. Heinz, Phys. Rev. Lett. **105**, 136805 (2010).
[7] J. Chen, N. Kuriyama, H.T. Yuan, H.T. Takeshita, T. Sakai, J. Am. Chem. Soc. **123**, 11813 (2001).
[8] K. Chang, W. Chen, ACS Nano**5**, 4720 (2011).
[9] Y.F. Li, Z. Zhou, S.B. Zhang, Z.F. Chen, J. Am. Chem. Soc. **130**, 16739 (2008).
[10] G. Seifert, H. Terrones, M. Terrones, G. Jungnickel, T. Frauenheim, Phys. Rev. Lett. **85**, 146 (2000).
[11] Y.V. Shtogun, L.M. Woods, J. Phys. Chem. C **113**, 4792 (2009).
[12] T.H. Cho, W.S. Su, T.C. Leung, W. Ren, C.T. Chan, Phys. Rev. B **79**, 235123 (2009).
[13] G. Kim, J. Bernholc, Y.-K. Kwon, Appl. Phys. Lett. **97**, 063113 (2010).
[14] G. Alfieri, T. Kimoto, Appl. Phys. Lett. **97**, 043108 (2010).
[15] S.L. Hu, Z.Y. Li, X.C. Zeng, J.L. Yang, J. Phys. Chem. C **112**, 8424 (2008).
[16] C.W. Chen, M.H. Lee, Y.T. Lin, Appl. Phys. Lett. **89**, 223105 (2006).
[17] H. Yilmaz, B.R. Weiner, G. Morell, Phys. Rev. B **81**, 041312 (2010).
[18] Y.Z. Wang, B.L. Wang, Q.F. Zhang, J.J. Zhao, D.N. Shi, S. Yunoki, F.J. Kong, N. Xu, J. Appl. Phys. **111**, 073704 (2012).
[19] Y.Z. Wang, B.L. Wang, Q.F. Zhang, D.N. Shi, S. Yunoki, F.J. Kong, N. Xu, J. Appl. Phys. **113**, 034301 (2013).
[20] A.J. Du, Z.H. Zhu, Y. Chen, G.Q. Lu, S.C. Smith, Chem. Phys. Lett. **469**, 183 (2009).
[21] Q.H. Liu, L.Z. Li, Y.F. Li, Z.X. Gao, Z.F. Chen, J. Lu, J. Phys. Chem. C **116**, 21556 (2012).
[22] K. Dolui, C.D. Pemmaraju, S. Sanvito, ACS Nano **6**, 4823 (2012).
[23] Q. Yue, S.L. Chang, J. Kang, X.A. Zhang, Z.Z. Shao, S.Q. Qin, J.B. Li, J. Phys.: Condens. Matter **24**, 335501 (2012).
[24] B. Delley, J. Chem. Phys. **92**, 508 (1990).
[25] B. Delley, J. Chem. Phys. **113**, 7756 (2000).
[26] J.P. Perdew, K. Burke, M. Ernzerhof, Phys. Rev. Lett. **77**, 3865 (1996).
[27] D.R. Hamann, M. Schluter, C. Chiang, Phys. Rev. Lett. **43**, 1494 (1979).
[28] W.F. Li, G. Zhang, M. Guo, Y.-W. Zhang, Nano Research **7**, 518 (2014).
[29] L.Z. Kou, C. Li, Z.H. Zhang, W.L. Guo, J. Phys. Chem. C **114**, 1326 (2010).
[30] J.S. Qi, X.F. Qian, L. Qi, J. Feng, D.N. Shi, J. Li, Nano Lett. **12**, 1224 (2012).
[31] J. Xiao, M.Q. Long, X.M. Li, H. Xu, H. Huang, Y.L. Gao, Sci. Rep. **4**, 4327 (2014).